18

The quest for high resolution phasing for large macromolecular assemblies exhibiting severe non-isomorphism, extreme beam sensitivity and no internal symmetry

Ada Yonath

18.1 Introduction

The translation of the genetic code into polypeptide chains is a fundamental life process. In rapidly growing bacterial cells the biosynthetic machinery constitutes about half of the dry weight of the cell, and the biosynthetic process consumes up to 80% of the cell's energy. Among the over 100 different compounds participating in the biosynthetic process is a giant riboprotein complex which has been studied crystallographically for quite some time: the ribosome, an unstable 2350 kDa assembly of many proteins and RNA of diverse structures. This universal organelle mediates the translation step of the biosynthetic process by catalysing the sequential polymerization of amino acids according to the blueprint, encoded in the mRNA [for recent reviews see Wilson and Noller (1998), Yonath and Franceschi (1998)].

A typical bacterial ribosome (called 70S) has a molecular weight of 2.3×10^6 Da. About one-third of its mass is comprised of some 58–73 different proteins, depending on its source. The remaining two-thirds is made of three chains of rRNA, with a total of about 4500 nucleotides. These are arranged in two independent subunits of unequal size which associate upon the initiation of protein biosynthesis. The large subunit has a mass of 1.45×10^6 Da. It contains 36–48 different proteins and two RNA chains (with a total of some 3000 nucleotides). The small subunit has a mass of 0.85×10^6 Da and it contains 21 proteins and an RNA chain of about 1500 nucleotides. Each of the two ribosomal subunits carries out different tasks and displays different properties. The large subunit catalyses the chemical reaction of the formation of the peptide bond and provides the path along which the nascent protein progresses. The range of functional activities of the small subunit is larger. It provides the site for the initiation of the translation step, facilitates the decoding of the genetic information and creates the fundamental feature of the *in vivo* initiation selection mechanism. Most of the aminoglycoside antibiotics that cause misreading of mRNA codons during translation, interact with it.

The observations that ribosomes can pack periodically and the hypothesis that these ordered forms are the physiological mechanism for temporary storage, aimed at preserving the integrity and activity of the ribosomes for an expected better future, stimulated us to attempt crystallization. Ribosomes from prokaryotes were chosen, as they are smaller and have been characterized biochemically in much greater detail than those from eukaryotes. They provide systems for *in vitro* crystallization independent of *in vivo* events influenced by environmental influences (e.g. stress, cold shocks, wrong diet) which might be difficult or impossible to control and to reproduce. They can also be produced in high purity and large quantities, essential for effective crystallographic studies. The key for obtaining diffracting crystals from ribosomal particles was the choice of the organism: halophilic or thermophilic bacteria; presumably because these ribosomes are more stable than those from eubacteria. A strong correlation between the activity of the ribosomes and the quality of their crystals was found. Furthermore, in all cases, except for some fragmentation of rRNA, the crystallized material retains its integrity and biological activity for long periods, in contrast to the short lifetime of isolated ribosomes in solution.

Crystals have been grown from ribosomes, their complexes mimicking defined stages in protein biosynthesis and their natural, mutated, selectively depleted and chemically modified subunits (Berkovitch-Yellin *et al.* 1992). Far beyond the initial expectations, two of these crystal forms, of the large subunits from *Haloarcula marismortui* (H50S) and of the small subunit from *Thermus thermophilus* (T30S), diffract currently to around 3 Å (Fig. 18.1). Although this resolution range may seem to be inferior to what is obtained from crystals of other large macromolecular complexes, for ribosomal crystals it should be considered rather high in view of their enormous size, which does not contain any internal symmetry, and the high level of their complexity.

It was found that the ribosomes are tough subjects for crystallographic analysis, primarily because they are composed of highly degradable RNA along with proteins, some of which may be loosely held. Table 18.1 shows that, in contrast to the common observations in macromolecular crystallography, the high resolution obtained from the ribosomal crystals is not necessarily linked to the diffraction of a high quality. Thus, the crystal-type diffracting to the highest resolution (H50S) yields the most problematic diffraction data. The efforts towards the elucidation of the structure of the ribosome and the problems (solved as well as unsolved) encountered over the years, are the subjects of this article.

18.1.1 *Crystals of the whole 70S ribosome*

These crystals, diffract to low resolution, presumably due to the inherent conformational heterogeneity of their preparations, as they are extracted directly from cells during their growth phase. However, crystals of a complex mimicking a defined functional state, containing T70S ribosomes, an oligomer of about 35 uridines and two charged tRNA molecules, diffract to a higher resolution than that obtained from purified 70S ribosomes [see Table 18.1 and Hansen *et al.* (1990)]. A further improvement of the resolution is expected from

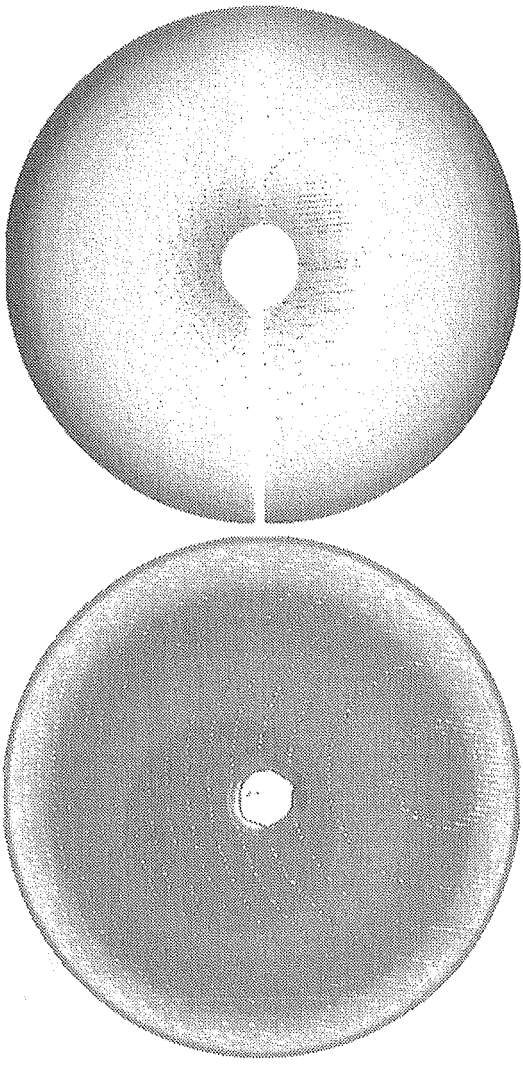

Fig. 18.1. *Top*: a 1° rotation diffraction pattern obtained from a crystal of treated small subunit from *Thermus thermophilus* (T30S), obtained at ID2/ESRF. *Bottom*: a 0.5° rotation diffraction pattern of a fresh crystal of H50S soaked in solution with 0.5 mM of W30, obtained in 20 s at the microfocus beamline (ID13) at ESRF (see Plate Section).

crystals programmed with mRNA of selected sequences. These complexes should eventually allow the mapping of the different conformations adopted by the ribosome while performing its function.

18.1.2 *The readiness of the large ribosomal subunit (50S) to crystallize*

This can be linked to its relative stability. Thus, 18 crystal forms have been grown from these particles, four of which were found to be suitable for crystallographic

Table 18.1. The quality of the ribosomal crystals

Source	Cell parameters (Å)	Resolution (Å)[a]	Isomorphism[b]	Beam sensitivity[c]	Spot shape[d]	Mosaicity[e]	Crystal shape and rigidity[f]
T70S[C]	524 × 524 × 306 $P4_12_12$	12/15	ok	U	ok	High	ok
T30S	407 × 407 × 176 $P4_12_12$	3.0/3.5	ok	High	ok	Rather high	Thin soft
T50S	495 × 495 × 196 $P4_12_12$	3.4/4.0	ok	U	ok	ok	ok
H50S	211 × 300 × 567 $C222_1$	2.7/3.2	Hardly any	Very high	Deformed elongated non-uniform	Very high	Problematic

T70S, T50S, T30S = the whole ribosome from *Thermus thermophilus* and its two subunits; H50S = the large subunit from *Haloarcula marismortui*.
[C] A complex of T70S ribosomes, two phe-tRNA^{phe} molecules and an oligomer of 35 uridines (as mRNA). The crystals of the pure T70S ribosome pack in the same crystal form but diffract only to 18/14 Å.
[a] The highest detectable/useful resolution. 'Useful' means 75% completeness (or higher) in the last shell.
[b] Isomorphism refers to native crystals grown from the same preparation. An 'ok' indicates reasonable isomorphism for above 50% of the crystals. 'Very bad': less than 10% of the crystals are isomorphous (defined by cell dimensions and/or the distribution of the average $\Delta F/F$ values vs resolution).
[c] Beam sensitivity at cryo-temperature, using bright synchrotron radiation beam.
[d] An 'ok' corresponds to 0.2–0.5° mosaic spread. 'Very high' may reach up to 3°.
[e] An 'ok' spot shape means that the reflections have a defined shape which corresponds to the shape of the crystals and to the cross-section of the beam. Elongated and undefined shape indicates, in addition to these properties, a high chance for interpenetration.
[f] An 'ok' means crystals of fairly isotropic dimensions which, when handled carefully, do not develop severe deformations. 'Problematic' means extremely thin crystals, built from readily sliding layers, which, even upon extremely careful handling may suffer from resolution loss and fragmentation.
U: Unknown or not well determined, since these crystals do not diffract to the resolution showing fast decay.

analysis at various levels of detail. The crystals of the halophilic large subunits (H50S) have been the target of extensive crystallographic analysis, since they diffract to almost atomic resolution, 2.5–2.7 Å (von Böhlen *et al.* 1991). However, although data collected carefully at intermediate resolution led to MIR phasing (Yonath *et al.* 1998), it was found that the undesired properties of this crystal form (Table 18.1) become more problematic and less tolerable with the increase of resolution. For instance, at the higher resolution ranges the crystal decay is expressed not only by loss of resolution, which can be monitored visually, but also in an invisible, albeit substantial, growth of the longest unit cell axis (Fig. 18.3). It is conceivable that each of the problems encountered could have been tolerated, but the combination of severe non-isomorphism, high radiation sensitivity, non-stable cell constants, non-uniform mosaic spread, uneven reflection shape and high fragility led in many cases to extreme difficulties even in the mere production of reliable data sets, let alone the construction and the interpretation of high resolution difference Patterson maps.

It should be mentioned that in each preparation there are some crystals that lead to reasonable mosaic spread (0.1–0.2°), non-deformed reflection spot shape and no additional patterns (resulting from layer sliding). Experience showed that the probability of detecting such crystals decreases with the increase of resolution (from 3–4% for those diffracting to 6–7 Å to 1–2% of the crystals yield high quality diffraction to higher limits, namely 2.7–3.3 Å). Combined with the very low level of isomorphism and the extreme sensitivity to irradiation, the above rather poor statistics hamper smooth and efficient high resolution phasing.

The 10–12 Å map (Fig. 18.2) is based primarily on the contribution of a strong derivative, Ta_6Br_{14}. This derivative led to a well defined, thus readily interpretable difference Patterson map at 7.5 Å (Fig. 18.2), even when all data with resolution below 12.5 Å were omitted. Consequently, its difference Fourier map enabled the positioning of the sites of two weaker derivatives, W12 and W17 (Table 18.2). The resolution of this map is currently being extended to 7 Å. The currently available intermediate map (at 8 Å) shows a higher connectivity and can be partially interpreted (to be published). Indeed, the Ta_6Br_{14} derivatized crystals diffract well to a resolution much higher than the limits currently set by us, owing to the above-described obstacles.

This MIR map may shed light on the odd combination of the properties of H50S. Thus, the extensive interparticle contacts that are concentrated in parts of the unit cell may account for the high resolution. However, in contrast to this dense packing, only a relatively small region, surrounded by a sizeable volume of solvent with dimensions that may reach over 200 Å in their longest direction, is involved in contacts between the two halves of the unit cell along the very long *c*-axis (567 Å) direction. Although still uncertain, it seems that the isolated contact network is made by two symmetry-related particles via RNA chains (Harms *et al.* 1999). As these interparticle contacts appear to be rather loose, we assume that they are partially mediated by the solvent. Hence, the influence of Mg and Cd ions on the rigidity of the crystals and their thickness may also be understood.

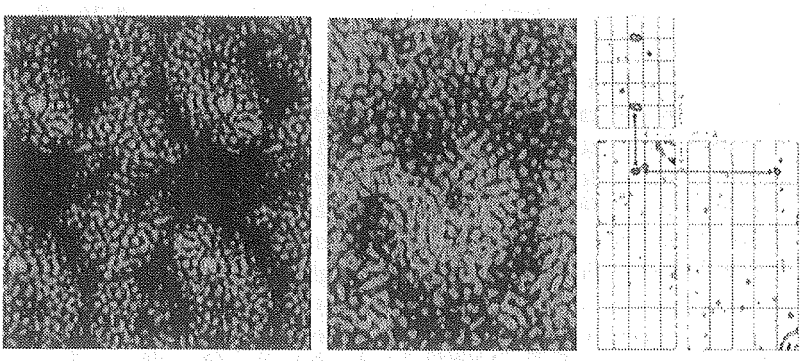

Fig. 18.2. *Left*: a part of the current 10–12 Å MIR map of H50S, showing the compact packing regions (around $z = 1/4$ and 3/4) as well as the isolated contact area along the z-axis. For clarity, two unit cells are shown along the y-direction (horizontal). The dense areas represent the position of the most occupied heavy atom site (at the interface between two subunits). *Middle*: the Ta_6Br_{14} difference Patterson map of H50S, including the data of the 7.5–12.5 Å resolution shell. The corresponding Harker peaks are shown by arrows. *Right*: a part of the map oriented to show the entrance to the main ribosomal internal tunnel (Yonath *et al.* 1987). More than 11 000 reflections were measured, and a total of 15 heavy atom sites of the three derivatives (Ta_6Br_{14}, W12 and W17, Table 18.2) were included. The positioning of the heavy atom sites was performed by a combination of difference Patterson and Fourier methods, based on the major position of Ta_6Br_{14}, found to be stable and consistent in all resolution ranges until 7.5 Å. Each heavy atom position was cross-verified and refined by MLPHARE with maximum likelihood. Since the contribution of the two W clusters was negligible beyond 10 Å, their scattering curve could be approximated by spherical averages of their corresponding radii (W18: 10 Å and W12: 8–9 Å). The Ta_6Br_{14}, however, was treated as in Knäblein *et al.* (1997) owing to its potential contribution to the higher resolution shells. Mean figure of merit: 0.32 (0.57 for centric); R_{cullis}: 0.76–0.97; phasing power: 0.98–1.15. The map was solvent flattened: one cycle, assuming 54% solvent (see Plate Section).

Table 18.2. Metal clusters

PIP = di-iododiplatinum (II) diethyleneamine
TAMM = tetrakis (acetoxymercuri)-methane
Ta_6Cl_{14}
$Ta_6Br_{14} \cdot 2H_20$
Nb_6Cl_{14}
$Ir_4(CO)_8R'_2R''$ **
$C_{22}H_{280}N_{24}O_{38}P_7Au_{11}$**
$W12Rh = CS_5H_xSiW_{11}O_{39}Rh^{III}CH_3COO(H)$**
$W30 = K_{14}(NaP_5W_{30}O_{110})31H_2O$
$W12 = K_5H(PW_{12}O_{40})nH_2O$
$W18 = (NH_4)_6(P_2W_{18}O_{62})14H_2O$
$W17Co = CoWLi17 = Cs_7(P_2W_{17}O_{61}Co(NC_5H_5))nH_2O$
$BuSnW17 = K_7[(buSn)(P_2W_{17}O_{61})]nH_2O$
$PhSnW15 = K_5H_4[(phSn)_3(P_2W_{15}O_{59})]nH_2O$
$BuSnW15 = K_5H_4[(buSn)_3(P_2W_{15}O_{59})]nH_2O$
$Na_{16}[(O_3PCH_2PO_3)_4W_{12}O_{36}]nH_2O$

**Should be used for covalent binding. R = $CH_2CH_2CONH_2$; R′ = $CH_2CH_2CONHCH_2$-CH_2CONH_2; bu = butyl; ph = phenyl.
For references see Weinstein *et al.* (1989), Thygesen *et al.* (1996), Knäblein *et al.* (1997), Lunger *et al.* (1997).

Such an unusual packing arrangement may be the reason for the low isomorphism of this crystal form, for the problematic morphology (plates reaching up to $0.5 \times 0.5\ mm^2$ with a typical thickness of a few microns in the direction of the *c*-axis), for the layer structure of the crystals, for the high tendency of these layers to slide relative to each other (causing multilattice diffraction patterns), for the changes in the *c*-axis that are introduced by irradiation (Fig. 18.3)

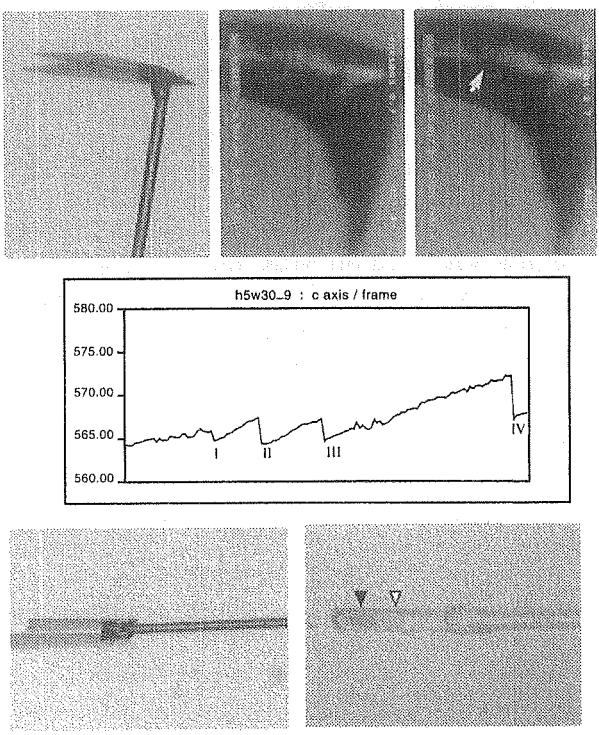

Fig. 18.3. *Top row*: (left) a perpendicular double spatula used for mounting H50S crystals; (Middle and Right) two photographs of the irradiated crystal, at the beginning of the experiment (the square shows the area being exposed) and after the decay of this position. Note that the irradiated region became dark (indicated by the arrow). *Middle row*: the 'fluctuating' *c*-axis. Data were collected sequentially from a crystal of H50S, mounted as shown on the right. The crystal size was $400 \times 380 \times 8\ \mu m$ and the beam cross-section $100 \times 100\ \mu m$. The initial resolution was higher than 3.2 Å (at the edge of the MAR detector). The loss of resolution was monitored by visual inspection, and when it reached 6–7 Å (points I, II, III), the crystal was translated to a new position. At the position marked IV the resolution limit is 9.5 Å. The region exposed last suffered from the decay of its neighbour even before its own exposure. While evaluating the data it was found that the crystal decay was accompanied by an increase in the *c*-dimension, from 564 to 572 Å. *Bottom row*: (left) a flat spatula, used for mounting T30S crystals; (right) a crystal of $300 \times 50 \times 30\ \mu m$, placed in a spatula similar to that shown on the left, was irradiated by a beam with a cross-section of $65\ \mu m$ at ID19/APS. The first position was at the far end of the spatula (black arrow) and translated once decayed (total 4°, 20 rotations 0.2° each) to the middle of the spatula (white arrow). There it was exposed for 15 s. The intact crystal was transparent. Note that the intensities of the 'burns' of the crystals are proportional to the exposure time (see Plate Section).

and for the penetration of very large clusters (e.g. W30, W18, W17, see Table 18.2) into the crystals. It should be mentioned that a similar packing arrangement was obtained independently by molecular replacement, exploiting the image reconstructed from T50S (Yonath *et al.* 1998; Harms *et al.* 1999). However, although this solution yields reasonable scores (i.e. 93% correlation with an *R*-factor of 27% for the region > 60 Å; and 48% correlation with an *R*-factor 42% for the region 30–90 Å), it is comparable to several other solutions. The use of the envelope of a ribosomal particle from one bacterium for determining the packing diagram of crystals grown from the same particle, but from a different source, is based on the assumption that at low resolution the gross structural features of prokaryotic ribosomes are rather similar. However, at higher resolution the validity of such studies is questionable and the loss in scores with the advance of resolution may be accounted for by the difference between T50S and H50S (the latter contains 12–14 additional proteins).

Three additional packing arrangements have previously been suggested for H50S crystals. The first was based on MIR and anomalous phase information, initially determined at 15 Å (Schlünzen *et al.* 1995). The second (Roth *et al.* 1996), the third (Ban *et al.* 1998) and the current (Yonath *et al.* 1998) seem to be rather similar not only in their packing scheme but also because both originate from non-MIR information (direct methods and molecular replacement, respectively) at 30 Å, and so far both could be validated only to low resolution limits, 10–12 Å.

Apart from the general concern regarding the domination of the phases determined by molecular replacement or similar procedures, relying solely on phase information originating from very low resolution information may be rather misleading. Thus, the extension of procedures developed for systems possessing extensive levels of internal non-crystallographic symmetry and/or for the use of heavy atom derivatives showing (potentially or in reality) phasing power extending near-molecular resolution (Jack *et al.* 1975), is not always justified. This is so especially when the non-MIR information is the main source for the determination of the heavy atom sites (using difference Fourier), and when the phasing power of these heavy atoms extends only to low resolution (i.e. 10–14 Å). In these resolution ranges the contribution of the non-crystalline material (the solvent) to the structure factors may reach the same order of magnitude as the contribution of the crystalline material. Therefore, the diffraction may be strongly influenced by the contribution of the solvent. Consequently, the chances that the heavy atom sites so determined may indeed represent changes in the solvent rather than in the structured material are non-negligible, even when they display acceptable phasing statistics (e.g. Schlünzen *et al.* 1995) and/or apparent anomalous signals.

This risk is especially high for the combination of ribosomal crystals with multitungsten clusters. In recent studies we have found that a significant amount of W clusters, in quantities much higher than those directly incorporated in the phasing procedure (i.e. detected in difference Patterson or Fourier maps) remain within the crystal environment even after applying an extensive washing procedure (12 times during 40–50 h). Thus, the number of W atoms found in

the washed crystals by inductively coupled plasma mass spectrometry as well as by atomic emission spectrometry, are equivalent to 18–20 clusters of W30 or to 25–27 clusters of W18 per ribosomal particle. Such large amounts of 'floating' W clusters are sufficient to generate measurable anomalous signals by contributing to the structure factors, as well as to introduce subtle non-isomorphism, which may not be detected as such in routinely treated diffraction data. It therefore remains to be seen whether the bases for these three structures (Schlünzen *et al.* 1995; Roth *et al.* 1996; Ban *et al.* 1998), i.e. the signals produced by these clusters at 12–15 Å, were a consequence of real derivatization, or of inherent or induced non-isomorphism or of the mere modification of the density of the crystal solvent.

In contrast to the marked tendency of large ribosomal subunits to crystallize, only one crystal form has so far been obtained from the *small ribosomal subunit* (Trakhanov *et al.* 1987; Yonath *et al.* 1988). For almost a decade this crystal form (T30S) yielded satisfactory data only to 12–15 Å (Schlünzen *et al.* 1995), although reflections were observed up to 7.3 Å. The low internal order of the crystals of the small ribosomal subunits was correlated with their marked instability, which reaches a higher level than that observed for the large subunits. For example, by exposing 70S ribosomes to a potent proteolytic mixture, the 50S subunits remained intact, whereas the 30S subunits were completely digested. Similarly, large differences in the integrity of the two subunits were observed while attempting the crystallization of functionally active 70S ribosomes, constructed from purified large and small subunits, then combined to form active ribosomes. It was found that the crystals obtained from these preparations consisted only of 50S subunits (Berkovitch-Yellin *et al.* 1992). This indicates that the self-affinity of the large subunits overcame their interactions with the small subunits to produce 70S particles not engaged in protein biosynthesis. It is noteworthy that at the end of this experiment, the supernatant of the crystallization drop did not contain intact small subunits, but instead their proteins and their fragmented RNA chain. Thus, while the large subunits crystallized, the small ones dissociated into their individual components.

Subtle modifications in the procedures of bacterial growth and crystal treatment led recently to diffraction of high quality at much higher resolution, 3–3.5 Å. Against all odds, the crystals of T30S are of a higher quality than any obtained from the large subunits, and display reasonable (though far from perfect) isomorphism (Table 18.1). Furthermore, data collected from T30S crystals under different conditions (stations and detectors): IP(MAR 345) at ID2-(ESRF), CCD at F1/CHESS and IP(MAR 300) at BW6/DESY, merged very well (R_{merge} 8–11%, compared to individual R_{merge} values of 6–9%). Large, medium-size and smaller metal compounds are being exploited for MIR and MAD phasing, leading typically to multisite binding which imposes extensive cross-verifications. This approach led to sufficient phasing power up to 6–6.3 Å resolution (limits currently dictated by the derivatized crystals) and allowed the construction of an interpretable electron density map (to be published).

18.2 Synchrotron radiation and crystal decay

The large unit cell dimensions and the extremely weak diffraction power do not permit any crystallographic preparative work, including crystal screening, to be performed on home generators, thus dictating absolute dependence of synchrotron radiation for all stages of structure determination. At ambient temperature, ribosomal crystals decay upon the first instance of irradiation. To overcome this unusual sensitivity, the concept of data collection at cryo-temperature was pioneered (Hope *et al.* 1989). Consequently, flash frozen ribosomal crystals can be irradiated by synchrotron radiation of moderate intensities (i.e. the bending magnet stations at DESY) at 85–95 K, with no observable radiation damage for periods sufficient for the collection of a complete data set at medium or low resolution (6–9 Å) and in exceptional cases even at 5 Å (Hope *et al.* 1989). However, even when the decay was not manifested in resolution loss, in many cases prominent damage has been observed at the outer resolution shells. This 'hidden' decay is detectable in the data quality, which becomes poorer with the progression of the irradiation, and is expressed in lower signal-to-noise ratios (e.g. from the original 9–10 to 2–3), higher R_{merge} values (e.g. from 0.06 to 0.17), fluctuations in the intraframe scaling factors between successive frames and frequent changes in the unit cell dimensions.

Because of the outstanding experimental demands of ribosomal crystallography, even the pre-freezing treatment must be performed with special care, although it introduces a higher level of complication. In attempts to maximize the useful resolution and to minimize the variation between crystals, procedures were developed for careful mounting of the crystals in a protective miniature double-layer thin glass spatula, and plunging them rapidly into liquid propane at its melting temperature (about 85 K). These double spatulas were found to be superior to the popular loops (Teng *et al.* 1994), although diffraction patterns of lower quality could also be collected from loop-mounted crystals. Thus, the double spatula accommodates the delicate properties of the ribosomal crystals: the extreme anisotropic morphology (one very thin dimension, of about 2–5 μm and two rather normal ones, of 200–400 μm), the notable softness and the high pliability, whereas crystals mounted in loops may float on the surface of the solvent bubble caught by the loop and bend around its concave shape. To address the hypothesis that the pre-freezing procedures may introduce apparent non-isomorphism, relatively large crystals were halved and each of its halves was flash-frozen separately. The two halves were positioned in the beam in a similar orientation, and data were collected around the cell axes of each part. Differences of magnitude similar to the experimental errors in the determination of all cell axes were observed.

It was firmly established that for collecting the higher resolution (2.5–6 Å) diffraction, high brilliance SR radiation (such as ID2 and ID13/ESRF or F1/CHESS) is essential. Unfortunately, such high brightness causes substantial radiation damage even at 15–95 K, within a period sufficient for the collection of a few rotations. The need to merge data from many crystals, coupled with the low level of isomorphism of the H50S crystals, makes it almost impossible to construct complete data sets even from native crystals. Since no improvement

was obtained by the addition of free-radical absorbers, or by using a He stream (at 15–20 K) during data collection, a procedure was designed for the irradiation of the crystals in parts, using a beam of a cross-section smaller than the crystal. This procedure led to useful medium resolution data, but the high resolution shells are still rather problematic, since, as mentioned above, the decay is expressed not only in loss of resolution, but also in gradual, albeit substantial increase of the C unit cell axis (Fig. 18.3), which occurs mainly at the higher resolution shells.

18.3 Elucidation of phases

The assignment of phases to the structure factor amplitudes is the most crucial, albeit most complicated step in structure determination. Clearly, for large macromolecular assemblies that cannot be subdivided by internal symmetry, the magnitude and the complexity of phasing is greatly increased and involves outstanding experimental demands.

18.3.1 *The derivatization agents: soaking experiments*

The commonly used methods for phase determination in biological crystallography, MIR, SIR and MAD, require the preparation of derivatives, usually by introducing electron-dense compounds into the crystalline lattice at a limited number of distinct locations while keeping the crystal parameters isomorphous with those of the native molecule. The most common procedure is to soak the crystals in solutions containing heavy atom compounds. Single heavy atoms have yielded useful high resolution phases for several large complexes. Among these are the viruses [e.g. Jack *et al.* (1995), Rossmann (1995)], the 371 K ATPase (Abrahams *et al.* 1994) and the 250 K $tRNA^{phe}$ synthetase and its complex with its cognate tRNA (Goldgur *et al.* 1997).

Owing to the enormous size of the ribosome, a large number of sites is required for generating accurately measured signals. Such multisite derivatives should be extremely difficult to locate in the unit cell. Alternatively, advantage can be taken of compact and dense compounds containing several heavy atoms linked directly to each other, or arranged in close proximity. However, in contrast to the availability of numerous single-atom agents, there are only a few stable water-soluble polymetallic compounds that may be suitable for the derivatization. Examples are heteropolyanions and multicoordination compounds usable for soaking experiments and monofunctional reagents of dense metal clusters, designed for covalent binding at specific sites prior to the crystallization (Table 18.2 and in Thygessen *et al.* 1995).

With the increase of resolution of the ribosomal crystals, medium-size compounds were tested. Among these is TAMM, which proved suitable for phasing data from crystals of rather large particles, such as the photosynthetic reaction centre (Deisenhofer *et al.* 1984), the nucleosome-core-particle (Luger *et al.* 1997), an iodotype–anti-idiotype complex (Bentley *et al.* 1990) and glutathione transferase (Reinemer *et al.* 1991), but could not be exploited in ribosomal crystallography either because of low solubility (H50S) or because it introduces severe

non-isomorphism (T30S and T50S). The situation with PIP, which was also used for phasing in some of the studies mentioned above (e.g. Luger *et al.* 1997) is unclear. It obviously did not introduce substantial non-isomorphism, but at the same time its phasing power was found to be lower than that obtained from smaller compounds, showing presumably that it decomposes in an uncontrolled fashion during the course of the experiment.

Ta_6Cl_{14} has recently become rather popular in macromolecular crystallography as it was shown to phase at different resolution ranges over a wide pH range. Thus, it was used for structure determination of ribulose-1,5-phosphate carboxylase/oxygenase (rubisco) and transketolase at 5.5 Å (Schneider and Lindquist 1994), as well as of the proteosome at 3.4 Å (Löwe *et al.* 1995) and at atomic resolution (Knäblein *et al.* 1997). This compound was found to be useful to various extents, for H50S, T50S and T30S crystal forms (see above and in Yonath *et al.* 1998).

18.3.2 *Quantitative attachment of heavy atom compounds*

Quantitative attachment to predetermined sites prior to crystallization ensures high occupancy. This approach requires complicated and time-consuming procedures, but is bound to yield indispensable information not only for phasing but also at later stages of map interpretation. Examples of compounds that may be bound are the clusters of undecatungsten (Wei *et al.* 1997), undecagold and tetra-iridium (Jahn 1989a,b), shown in Table 18.2.

The feasibility of phasing by specifically bound heavy atoms has been proven in several cases, including the nucleosome-core-particle (Luger *et al.* 1997), as well as for low resolution derivatization of B50S, performed with a monofunctional reagent of an undecagold cluster (Weinstein *et al.* 1989; Bartels *et al.* 1995).

The studies on the structure of the nucleosome-core-particle are illuminating. This 206 kDa particle consists of 146 base pairs of DNA wrapped around an internal core, composed of an octamer made of two copies of four histones. Since the fine characteristics of the structure of each individual nucleosome-core is dictated by the sequence of the incorporated DNA, which varies as a function of its position on the genome, crystals obtained from naturally occurring nucleosome-core-particles diffract at best to only 7 Å (Richmond *et al.* 1984). In order to decrease the natural crystal variability, a semi-artificial nucleosome-core-particle was designed, consisting of genetically produced wild-type or mutated histones together with a fragment of 146 base pairs, synthesized with a defined sequence. Thus, in addition to the provision of a homogenous population, the use of recombinant nucleosome-cores facilitated the insertion of exposed cysteines at selected sites on the surface of the histone proteins.

This elegant and logical approach cannot be adopted for the derivatization of the ribosomes, since so far all fully reconstructed particles did not yield crystals that diffracted well. This was rather unexpected since functionally active ribosomes can be reconstituted *in vitro* from isolated ribosomal components, indicating that the information required to obtain the active quaternary structure resides within them. It is conceivable that the *in vitro* reconstitution pathways lead to slight deviations from the natural conformation, since the conditions under which the reconstitution is performed *in vitro* are dramatically different

from the physiological events. For example, the *in vitro* assembly of the ribosome requires 90 min, whereas the *in vivo* process is completed within 3 min. These slight conformational differences can be tolerated and induced to form the correct active sites by their substrates, but are sufficiently severe to prohibit quality crystallization. Therefore the pre-crystallization heavy atom binding is limited either to the available sites on the native particles (there is one exposed cysteine on T30S and none on H50S) or to the genetic creation of potential binding sites on selected ribosomal proteins, those that can be quantitatively and reversibly detached from the ribosome under mild conditions [there are four such proteins in H50S and eight in T30S (Sagi *et al.* 1995)].

An example is in the studies exploiting a mutant of *Bacillus stearothermophilus*, lacking one ribosomal protein, BL11. The mutated 70S ribosomes and 50S subunits formed three-dimensional crystals and two-dimensional sheets under the conditions used for crystallizing the wild-type particles. Thus, the absence of BL11 does not cause gross conformational changes in the ribosomal particles, and it is not crucial for the interparticle interactions forming the crystallographic network. Protein BL11 is a ribosomal component that undergoes conformational changes upon isolation from the particle. Thus, when incorporated into the ribosome, its single free –SH group is exposed and chemically reactive. In isolation, however, this group is not reactive unless the protein is denatured. The gold cluster was quantitatively bound to isolated BL11 under denaturing conditions, and the modified protein was incorporated in the core particles, to form a specific and quantitative derivative. To place the size of the clusters in perspective, we note that the molecular weight of the undecagold cluster (6200 Da) is more than a third of the molecular weight of BL11 (15 500 Da) and its diameter, 22 Å, approaches three-fourths of the end-to-end dimension of lysozyme.

An obvious target for attachment of heavy atom clusters to ribosomal particles is tRNA. To facilitate co-crystallization of tRNA with ribosomal particles, we have determined conditions for stoichiometric binding of tRNA to ribosomal particles. One of these complexes mimics a defined state in the process of protein biosynthesis, composed of the 70S ribosome, a short segment of mRNA and two molecules of charged tRNA (Hansen *et al.* 1990). The undecagold cluster was covalently attached to $tRNA^{phe}$ at base 47. The modified tRNA molecule binds to the ribosome and can be aminoacylated by its cognate synthetase. Furthermore, it seems that the undecagold cluster did not introduce large perturbations into the ribosomal structure, as crystals of the complex containing the modified $tRNA^{phe}$ diffracted to resolution comparable to that obtained from the complex containing the native tRNA molecule.

In conducting proper isomorphous replacement experiments, the low level of isomorphism of H50S crystals dictated the exposure of many crystals in order to construct complete either native or derivatized data sets. A larger number is needed for the selection of rather isomorphous pairs. Thus, 27 data sets were constructed from data collected from 76 native and derivatized crystals, until four of them were found to exhibit reasonable isomorphism at about 7 Å. As described above, similar studies performed on T30S progressed somewhat more smoothly. In this case, large and medium-size compounds alongside

smaller salts were exploited. In both cases, some of the difference Patterson maps were too complicated to be interpreted in the conventional way. Extensive alternations between difference Patterson and Fourier maps were performed to allow heavy atom site location. This sophisticated approach was later combined with careful analysis and led to preliminary indications for sufficient phasing power.

18.3.3 *Phasing by MAD*

MAD phasing should eliminate the dependence on isomorphism, provided that all the data can be collected at a few wavelengths from a single crystal. Owing to the severe radiation decay of the ribosomal crystals, this requirement cannot be fulfilled, but it is anticipated that even partial high resolution phase information obtained from individual crystals should be more useful than that expected to be obtained from difference Patterson maps. The suitability of this method for ribosomal crystallography is currently being assessed and a word of caution is due, since the anticipated anomalous signals may be of the same order of magnitude as the changes in structure factors induced by the decay of the crystals. MAD studies exploiting selenium recently gained a lot of popularity in protein crystallography. For obtaining selenated halophilic ribosomal particles, a methionine-dependent strain was constructed (M. Mevarech, private communication). The 50S subunits of this strain yield crystals that may be of a higher quality than those grown from the problematic H50S wild-type (Fig. 18.4). The exact numbers of methionines in T30S and H50S are still to be determined, since only a part of the sequences of the ribosomal proteins from these sources is known. Their estimated numbers (25 and 55, respectively) may not be sufficient to provide measurable signals, therefore efforts are being made to increase their amounts by genetic techniques (Franceschi *et al.* 1993).

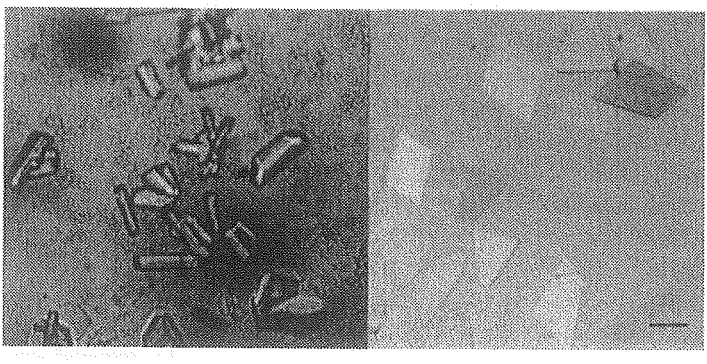

Fig. 18.4. *Left*: Crystals of large ribosomal subunits from strain H2 grown under conditions somewhat milder than those used for H50S (1.45 instead of 1.6 M KCl); *right*: those of H50S. Bars: 0.2 mm (see Plate Section).

18.3.4 *Molecular replacement*

Molecular replacement is based on manoeuvring the positioning of a known model in the unit cell of the unknown structure until the calculated structure factors match best the observed ones. The rotation–translation searches have been performed, initially by exploiting models obtained from electron micrographs of tilt series of negatively stained crystalline arrays of 70S ribosomes and 50S subunits from *B. stearothermophilus* (Yonath *et al.* 1987; Arad *et al.* 1987). These were used despite their rather low (28–40 Å) resolution, since key functional features, such as the site of protein synthesis and the path of the nascent chain, were observed in them for the first time.

Higher resolution images (16–25 Å) have recently been obtained by angular reconstructions of single ribosomal particles embedded in vitreous ice. As similar images, resembling the views observed by traditional electron microscopy and containing the features revealed in the crystalline arrays, were obtained independently by two groups (Stark *et al.* 1995; Frank *et al.* 1995), they seem to be reliable. To enhance the chances for elucidating the correct packing arrangements of the ribosomal crystals, particles of the same preparations which yielded the best T50S and T70S crystals (Table 18.1) have been subjected to reconstruction at 18 and 26 Å resolution, respectively (Harms *et al.* 1999). In both cases, a unique solution was obtained in the rotation–translation studies showing no collisions or short contacts, with $R_{\text{merge}}(I)$ of 42% and 46% and correlations of 75% and 79%, respectively (Figs 18.5 and 18.6).

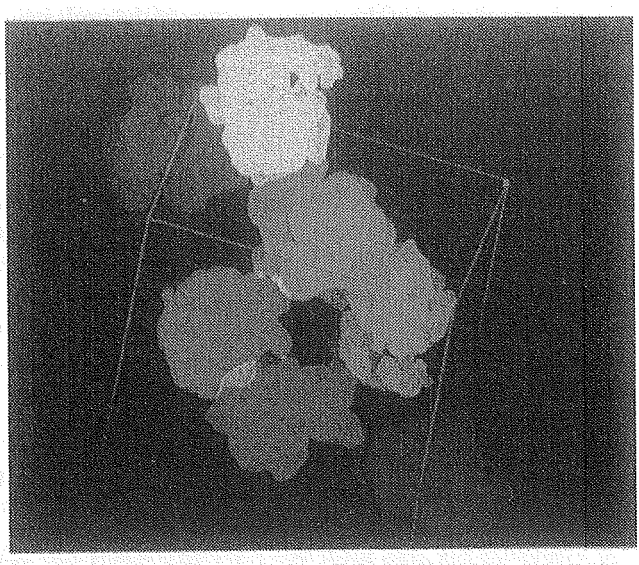

Fig. 18.5. The packing diagram of the crystallographic unit cell of whole ribosome (T70S), assembled by positioning the 26 Å electron microscope model in the crystallographic unit cell according to the most prominent result of the molecular replacement search, and applying the eight symmetry operations. Data were collected at BW6/DESY to 17 Å resolution (see Plate Section).

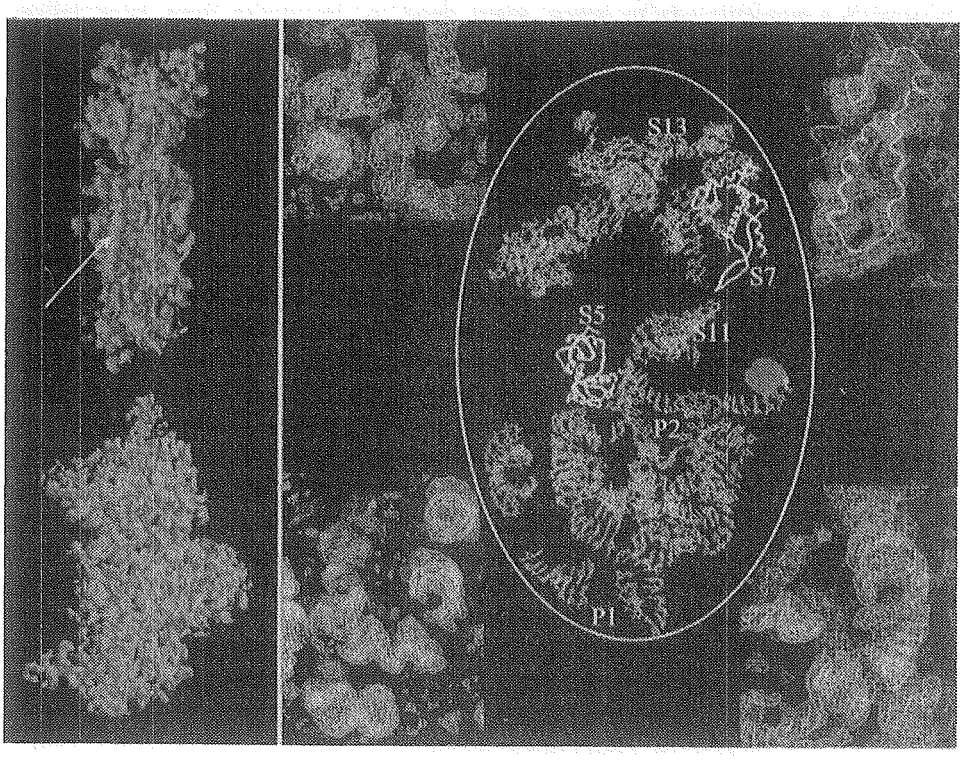

Fig. 18.6. *Left*: Two orthogonal views of the overall structure of the small subunit, as extracted from the 4.5 Å map. The arrow points to an exceptionally long dense region, suitable for hosting a double-helical RNA chain that may be interpreted as helix 44 in the model of the 16S RNA (Müller and Brimacombe 1997). For orientation, the location of the tail of the cDNA complementary to the 3′ end of the 16S RNA is shown in red on both sides (here and on the *Right* side). *Right*: Part of the 16S RNA chain so far traced in the 4.5 Å map of T30S is shown within the white ellipse. The position of the centre of mass of the TAMM molecules that were bound to the mRNA analog is shown as a red sphere (artificially enlarged). The locations of proteins TS5, TS7 are represented by their backbone structure, as determined crystallographically. Two tentative locations for protein TS15 are marked P1 and P2. The positions of the exposed cysteines of proteins TS11 and TS13 are marked by their numbers (see Plate Section).

Electron density maps were constructed from the observed crystallographic structure factor amplitudes and calculated phases, as well as from the observed amplitudes and the combination of the rotation search phases with those determined by SIRAS from crystals soaked in a solution of Ta_6Br_{14}, performed since a reasonable correlation was found between them (Fig. 18.6). An examination of the relation between the packing arrangement and the positions of the two most prominent Ta_6Br_{14} sites showed that one of them is located between two particles and the second in a small 'nest' within the particle (Fig. 18.6).

18.3.5 *Isolated ribosomal components and* in situ *complexes*

The immense difficulties anticipated (and encountered) in the determination of the structure of intact ribosomal particles has led to a parallel approach, focusing on isolated ribosomal components. For over a decade the yield of this approach was rather poor, but the substitution of the *E. coli* ribosome, which used to be the favoured research object, by more robust particles (e.g. from thermophilic bacteria), the employment of genetic techniques and the introduction of three-dimensional NMR spectroscopy, have resulted in major accomplishments in the determination of the molecular structure of an impressive number of ribosomal proteins (reviewed in Liljas and Al-Karadaghi 1997; Hosaka *et al.* 1997; Wimberly *et al.* 1997) as well as RNA fragments (Betzel *et al.* 1994; Puglisi *et al.* 1997; Dallas and Moore 1997; Correll *et al.* 1997). It remains to be seen whether the structures determined in isolation bear resemblance to the *in situ* situation. It is widely assumed that the inherent conformation is maintained despite changes in the environment. However, recent results challenge this assumption, as a significant discrepancy has been observed between the structure of a crystalline ribosomal protein and its NMR solution (Chlemons *et al.* 1998). Clearly, some of the structures of individual ribosomal components should not differ from their *in situ* state. These should be instrumental for the interpretation of the electron density map of the entire ribosomal particles, as they may provide useful markers.

Conformational readjustments have been predicted to be associated with the creation of the *in situ* microenvironment within the ribosome. It was widely assumed that the ribosomal components which undergo the main conformational changes are the rRNA molecules. The observation that flexible loops in ribosomal proteins become ordered upon binding to rRNA, indicates that changes in the protein conformation may also be essential for the assembly of the ribosome. At the same time it is anticipated that, provided the association with the *in situ* closest neighbours is maintained, isolated internal ribosomal complexes are likely to keep their natural conformations in solution. Assuming that some of the structures of the isolated complexes and single components indeed reflect the *in situ* situation, the crystal structures of these complexes may provide phase information in molecular replacement studies. They should also be instrumental in the interpretation of the electron difference maps, providing 'flags' and 'markers'.

18.4 Discussion, conclusions and perspectives

This is an exciting time in biological crystallography as projects that were considered beyond our reach until not too long ago, are currently being carried out. One of the most striking examples is ribosomal crystallography, which underwent dramatic progress since the submission of this chapter. As mentioned above, these studies required the pioneering of revolutionary concepts and sophisticated techniques, not only because ribosomes are giant assemblies with

no internal symmetry, but also because their crystals are extremely delicate, radiation sensitive, of rather low isomorphism and frequent polymorphism (Makowski *et al.* 1997; von Böhlen *et al.* 1991; Ban *et al.* 1999). Nevertheless, the approaches developed to minimize the harm caused by these negative properties, together with the increasing availability of bright synchrotron radiation beams coupled with reliable area and CCD detectors, led to spectacular results. Among those are (in decreasing order of resolution) a 7.5 Å map of functional complexes of 70S ribosome (Cate *et al.* 1999), a 5 Å map of the halophilic large subunit (Ban *et al.* 1999), a 5.5 Å map of the thermophilic small subunit (Clemons *et al.* 1999), and a 4.5 Å map of the small subunit, containing either chemical markers or functional analogs (Tocilj *et al.* 1999).

The 4.5 Å study of the small subunits is of great importance because it shows clearly that the border of 5 Å can be crossed. This is a major breakthrough since below 5 Å resolution complete data sets can be collected from single crystals, whereas the bright beam that is essential for collecting the higher resolution shells causes severe radiation decay. Consequently the data are more problematic and several crystals are required in order to produce complete data sets, a task that was found to be extremely demanding because of the severe non-isomorphism of some of the ribosomal crystal systems (i.e. H50S).

The strategy that proved suitable for phasing of all crystal systems is based on the determination of an initial phase set at very low resolution, followed by its extension by experimental and/or computational methods. For this aim, molecular replacement exploiting cryo EM reconstructions was performed successfully for H50S (Ban *et al.* 1999), T50S (Yonath and Franceschi 1998) and for the whole ribosome from *T. thermophilus*, T70S (Cate *et al.* 1999; Harms *et al.* 1999): however, for T30S these attempts were found not suitable, presumably because of the high conformational variability (Stark *et al.* 1995; Frank *et al.* 1995; Gabashvili *et al.* 1999; Harms *et al.* 1999; Wang *et al.* 1999). In this case the initial set of phases was obtained by using heavy atom clusters (Clemons *et al.* 1999; Tocilj *et al.* 1999).

So far, all attempts at interpreting the ribosomal electron density maps are based fully or partially on placements of structures of ribosomal components or of similar molecules, guided by the available non-crystallographic structural information obtained by electron microscopy, neutron scattering, footprinting, modelling and biochemical experiments [for a review, see Müller and Brimacombe (1997)]. The building blocks used for tracing the map were constructed from known RNA motifs or from the ribosomal proteins whose structures have been determined crystallographically or by NMR.

Placement of structures determined at high resolution in medium resolution maps requires special concern, as considerable uncertainties are associated with such attempts. In the case of the ribosome there are further potential ambiguities, since most of its individual components are built from common motifs (Liljas and Al-Karadaghi 1997; Ramakrishnan and White 1998). Also, at low or medium resolution, molecular mimicries (Nyborg *et al.* 1996) may mislead the differentiation between proteins and RNA regions. In addition, most of the ribosomal components possess non-negligible conformational variability that

may lead to misinterpretations, since their structures are likely to be influenced by the *in situ* ribosomal environment.

An exceptional case is the 4.5 Å map of small subunit (Tocilj *et al.* 1999) since heavy atom markers were used for its unbiased interpretation. These allowed independent positioning of ribosomal components as they attached to known chemically active ribosomal moieties or to carriers with a high affinity to specific locations in the 30S subunit, such as antibiotics or DNA oligomers, complementary to exposed single stranded RNA. Thus, post-crystallization activation by controlled heating led to higher proportions of satisfactorily diffracting crystals and enabled almost quantitative binding of compounds participating in protein biosynthesis or their analogs. In this way, close to stoichiometric hybridization with mercurated cDNA oligomers was achieved, despite their large-size, which may reach 70 Å in length.

Targeting the 16S RNA region, where mRNA docks to allow the formation of the initiation complex by a mercurated mRNA analog, led to the characterization of its vicinity (Weinstein *et al.* 1999; Auerbach *et al.* 1999; Bartels *et al.* 1999; Bashan *et al.* 1999; Tocilj *et al.* 1999). This region of the 16S chain is known to be rather flexible and may adopt several conformations and it is likely that the high quality diffraction obtained from the crystals derivatized by this oligomer results from stabilization of the flexible 3′ arm of the 16S RNA in a fashion similar to its binding to mRNA.

Similarly, heavy atom clusters (a tetrairidium and a tetramercury compound) covalently bound to the exposed sulphydryls of two ribosomal proteins, S11 and S13, were used to reveal their position in difference Fourier maps (Weinstein *et al.* 1999; Auerbach *et al.* 1999). Interestingly, the location of one of the two proteins, S13, found this way is in reasonable agreement with that suggested by neutron scattering (Moore *et al.* 1985), immunoelectron microscopy (Stöffler and Stöffler-Meilicke, 1986) and modelling based on cross-linking and enzymatic data (Müller and Brimacombe 1997). For protein S11 the situation is somewhat different. Its position in the electron density map is in accord with that proposed by electron microscopy and by modelling, but differs from that obtained by neutron scattering, by a distance larger than the expected diameter of this protein.

Despite the difficulties with molecular replacement, the overall structure of the small ribosomal subunit, as seen at 4.5 Å in the map, is remarkably similar to most of the electron microscopy reconstructions of this particle at its functionally active conformation. It shows the recognizable small subunit features, including the traditional division into three main parts: a rather large head, a short neck and a bulky lower body (Stark *et al.* 1995; Frank *et al.* 1995; Gabashvili *et al.* 1999). It contains elongated dense features as well as lower-density globular regions. In the latter, proteins S5 and S7 were placed visually. Suitable host regions for the fold of protein S15 were detected in several positions, all at a significant distance from the location of this protein in the neutron scattering map (Fig. 18.6).

The level of detail of some of the ribosomal electron-density maps, the ability to insert specific markers and the availability of crystals of functional complexes

that diffract to rather high resolution (3–3.5 Å) indicate that the elucidation of the molecular structure of the ribosomes is no longer so far away.

Acknowledgements

We express our exceptional gratitude to the late Prof. H.G. Wittmann with whom these studies were initiated, to Drs M. Pope, W. Preetz and W. Jahn who gave us generous gifts of heavy atom clusters and to the team working with us on this project. The studies presented here were performed at the Weizmann Institute, Rehovot, the Max-Planck Research Unit in Hamburg and the Max-Planck Institute for Molecular Genetics in Berlin. Data were collected at EMBL and MPG lines at DESY; F1/CHESS, Ithaca, NY; ID2, ID13, D2AM/ESRF/Grenoble; ID19/APS/ARGONNE,IL; PF/KEK, Tsukuba, Japan. Support was provided by the Max-Planck Society, the US National Institute of Health (NIH GM 34360), the German Ministry for Science and Technology (BMBF 05-641EA) and the Kimmelman Center for Macromolecular Assembly at the Weizmann Institute. A.Y. holds the Martin S. Kimmel Professorial Chair.

Abbreviations

tRNA, rRNA and mRNA stand for transfer, ribosomal and messenger RNA, respectively. r-proteins are ribosomal proteins. 70S, 50S, 30S: the whole ribosome and its two subunits. A letter as a prefix represents the bacterial source: E: *E. coli*; B: *Bacillus stearothermophilus*; T: *Thermus thermophilus*; H: *Haloarcula marismortui*. 5S RNA, the shortest RNA chain in the large ribosomal subunit.

References

Abrahams, JP, Leslie, AGW, Lutter, R and Walker, JE (1994). *Nature*, **370**, 621–628.

Arad, T, Piefke, J, Weinstein, S, Gewitz, HS, Yonath, A and Wittmann, HG (1987) *Biochimie*, **69**, 1001–1006.

Auerbach, T, Pioletti, M, Avila, H, Anagnostopoulos, K, Weinstein S, Franceschi, F and Yonath, A (1999). *Biomolecular Structure and Dynamics* (in press).

Ban, N, Freeborn, B, Nissen, P, Penczek, P, Grassucci, RA, Sweet, R, Frank, F, Moore, P and Steitz, T (1998). *Cell*, **93**, 1105–1115.

Ban, N, Nissen, P, Capel, M, Moore P and Steitz, T (1999). *Nature*, **400**, 841–847.

Bartels, H, Bennett, WS, Hansen, HAS, Eisenstein, M, Weinstein, S, Müssig, J, Volkmann, N, Schlünzen, F, Agmon, I, Franceschi, F and Yonath, A (1995). *Biopolymers*, **37**, 411–419.

Bartels, H, Glühmann, M, Janell, D, Schlünzen, F, Tocilj, A, Bashan, A, Levin, I, Hansen, HAS, Harms, J, Kessler, M, Pioletti, M, Auerbach, T, Agmon, I, Avila, H, Simitsopoulou, M, Weinstein, S, Peretz, M, Bennett, WS, Franceschi, F and Yonath, A (1999). *Cellular and Molecular Biology* (in press).

Bashan, A, Pioletti, M, Bartels, H, Janell, D, Schlünzen, F, Glühmann, M, Levin, I, Harms, J, Hansen, HAS, Tocilj, A, Auerbach, T, Avila, H, Anagnostopoulos, K, Simitsopoulou, M, Peretz, M, Bennett, WS, Agmon, I, Kessler, M, Weinstein, S, Franceschi, F and Yonath, A (1999). *ASM publications* (in press).

Bentley, GA, Boulot, G, Riottot, MM and Poljak, RJ (1990). *Nature*, **348**, 254–257.
Berkovitch-Yellin, Z, Bennett, WS and Yonath, A (1992). *Critical Reviews in Biochemistry and Molecular Biology*, **27**, 403–444.
Betzel, C, Lorenz, S, Fürste, JP, Bald, R, Zhang, M, Schneider, R, Wilson, KS and Erdmann, VA (1994). *FEBS Letters*, **351**, 159–164.
von Böhlen, K, Makowski, I, Hansen, HAS, Bartels, H, Berkovitch-Yellin, Z, Zaytzev-Bashan, A, Meyer, S, Paulke, C, Franceschi, F and Yonath, A (1991). *Journal of Molecular Biology*, **222**, 11–15.
Cate, JH, Yusupov, MM, Yusupova, GZ, Earnest, TN and Noller, HF (1999). *Science*, **285**, 2095–2104.
Clemons, WM, Davies, C, White, S and Ramakrishnan, V (1998). *Structure*, **6**, 429–438.
Clemons, WM, May, JLC, Wimberly, BT, McCutcheon, JP, Capel, MS and Ramakrishnan, V (1999). *Nature*, **400**, 833–840.
Correll, CC, Freeborn, B, Moore, PB and Steitz, TA (1997). *Cell*, **91**, 705–712.
Dallas, A and Moore, PB (1997). *Structure*, **5**, 1639–1653.
Deisenhofer, J, Epp, O, Miki, K, Huber, R and Michel, H (1984). *Journal of Molecular Biology*, **180**, 385–398.
Frank, J, Zhu, J, Penczek, P, Li, Y, Srivastava, S, Verschoor, A, Radamacher, M, Grassucci, R, Lata, AK and Agrawal, RK (1995). *Nature*, **376**, 441–444.
Franceschi, F, Weinstein, S, Evers, U, Arndt, E, Jahn, J, Hansen, HAS, von Böhlen, K, Berkovitch-Yellin, Z, Eisenstein, M, Agmon, I, Thygesen, J, Volkmann, N, Bartels, H, Schlünzen, F, Bashan, A, Sharon, R, Levin, I, Dribin, A, Sagi, I, Choli-Papadopoulou, T, Tsiboly, P Kryger, G, Bennett WS and Yonath, A (1993). *The Translational Apparatus*, ed. Nierhaus, K, Plenum Press. pp. 397–406.
Gabashivili, IS, Agrawal, RK, Grassucci, R and Frank, J (1999). *J. Mol. Biol.*, **286**, 1285–1291.
Goldgur, Y, Mosyak, L, Reshetnikova, L, Ankilova, V, Lavrik, O, Khodyreva, S and Safro, M (1997). *Structure*, **5**, 59–68.
Hansen, HAS, Volkmann, N, Piefke, J, Glotz, C, Weinstein, S, Makowski, I, Meyer, S, Wittmann, HG and Yonath, A (1990). *Biochemical and Biophysical Acta*, **1050**, 1–5.
Harms, J, Tocilj, A, Levin, I, Agmon, I, Kölln, I, Stark, H, van Heel, M, Cuff, M, Schlünzen, F, Bashan, A, Franceschi, F and Yonath, A (1999). *Structure*, **7**, 931–941.
Hope, H, Frolow, F, von Böhlen, K, Makowski, I, Kratky, C, Halfon Y, Danz, H, Webster, P, Bartels, K, Wittmann, HG and Yonath, A (1989). *Acta Crystallographica*, **B45**, 190–199.
Hosaka, H, Nakagawa, A, Tanaka, I, Harada, N, Sano, K, Kimura, M, Yao, M and Wakatsuki, S (1997). *Structure*, **5**, 1199–1208.
Jack, A, Harrison, SC and Crowther, RA (1975). *Journal of Molecular Biology*, **97**, 163–172.
Jahn, W (1989a). *Zeitschrift für Naturforschung*, **44b**, 79–82.
Jahn, W (1989b). *Zeitschrift für Naturforschung*, **44b**, 1313–1322.
Knäblein, J, Neuefeind, T, Schneider, F, Bergner, A, Messerschmidt, A, Löwe, J, Steipe, B and Huber, R (1997). *Journal of Molecular Biology*, **270**, 1–7.
Liljas, A and Al-Karadaghi, S (1997). *Nature Structural Biology*, **4**, 767–771.
Löwe, J, Stock, D, Jap, B, Zwickl, P, Baumeister, W and Huber, R (1995). *Science*, **268**, 533–539.
Luger, K, Mäder, AW, Richmond, RK, Sargent, DF and Richmond, TJ (1997). *Nature*, **389**, 251–260.
Makowski, I, Frolow, F, Saper, MA, Shoham, M, Wittmann, HG and Yonath, A (1987) *J. Mol. Biol.*, **193**, 819–821.

Moore, PB, Capel, MS, Kjeldgaard, M and Engelman, DM (1985). in *Structure, Function & Genetics of Ribosomes*, (Hardesty, B and Kramer, G, eds) Springer Verlag, Heidelberg & NY pp. 87–100.

Müller, F and Brimacombe, R (1997). *J. Mol. Biol.*, **271**, 524–544.

Nyborg, J, Nissen, P, Kjeldgaard, M, Thirup, S, Polekhina, G, Clark, BFC and Reshetnikova, L (1996). *Trends in Biochemical Sciences*, **21**, 81–82.

Puglisi, EV, Green, R, Noller, HF and Puglisi, JD (1997). *Nature Structural Biology*, **4**, 775–778.

Ramakrishnan, V and White, SW (1998). *Trends in Biochemical Sciences*, **3**, 208–212.

Reinemer, P, Dirr, HW, Ladenstein, R, Schäffer, J, Gallay, O and Huber, R (1991). *EMBO Journal*, **10**, 1997–2005.

Richmond, TJ, Finch, JT, Rushton, B, Rhodes, D and Klug, A (1984). *Nature*, **311**, 532–537.

Rossmann, MG (1995). *Current Opinion in Structural Biology*, **5**, 650–659.

Roth, M, Pebay-Peyroula, E, Bashan, A, Berkovitch-Yellin, Z, Agmon, I, Franceschi, F, Lewit-Bentley, A and Yonath, A. (1996). *Biological Structure and Dynamics, Proceedings of the 9th Conversation*, Sarma, RH and Sarma, MH, eds, p. 15.

Sagi, I, Weinrich, V, Levin, I, Glotz, C, Laschever, M, Melamud, M, Franceschi, F, Weinstein, S and Yonath, A (1995). *Biophys. Chem.*, **55**, 31–41.

Schlünzen, F, Hansen, HAS, Thygesen, J, Bennett, WS, Volkmann, N, Levin, I, Harms, J, Bartels, H, Zaytzev-Bashan, A, Berkovitch-Yellin, Z, Sagi, I, Franceschi, F, Krumbholz, S, Geva, M, Weinstein, S, Agmon, I, Böddeker, N, Morlang, S, Sharon, R, Dribin, A, Maltz, E, Peretz, M, Weinrich, V and Yonath, A (1995). *Journal of Biochemistry and Cell Biology*, **73**, 739–749.

Schlünzen, F, Kölln, I, Janell, D, Glühmann, M, Levin, I, Bashan, A, Harms, J, Bartels, H, Auerbach, T, Pioletti, T, Avila, H, Anagnostopoulos, K, Hansen, HAS, Bennett, WS, Agmon, I, Kessler, M, Tocilj, A, Peretz, M, Weinstein, S, Franceschi, F and Yonath, A (1999). *J. Syn. Radiation*, **6**, 928–941.

Schneider, G and Lindquist, Y (1994). *Acta Crystallographica*, **D50**, 186–192.

Stark, H, Mueller, F, Orlova, EV, Schatz, M, Dube, P, Erdemir, T, Zenin, F, Brimacombe, R and Van Heel, M (1995). *Structure*, **3**, 815–914.

Stöffler, G and Stöffler-Meilicke, M (1986). In *Structure, Function and Genetics of Ribosomes*, (Hardesty, B and Kramer, G, eds) Springer Verlag, Heidelberg and NY. pp.28–46.

Tocilj, A, Schlünzen, F, Janell, D, Glühmann, M, Hansen, HAS, Harms, J, Bashan, A, Bartels, H, Agmon, I, Franceschi, F and Yonath, A (1999). *PNAS* (in press).

Trakhanov, SD, Yusupove, MM, Agalarov, SC, Garber, MB, Ryazantsev, SN, Tichenko, SV and Shirokov, VA (1987). *FEBS Letters*, **220**, 319–323.

Teng, TY, Schildkamp, W, Dolmer, P and Moffat, K (1994). *Journal of Applied Crystallography*, **27**, 133–137.

Thygesen, J, Weinstein, S, Franceschi, F and Yonath, A (1996). *Structure*, **4**, 513.

Wang, R, Alexander, RW, VanLoock, M, Vladimirov, S, Bukhtiyarov, Y, Harvey, SC and Cooperman, BS (1999). *J. Mol. Biol.*, **286**, 521–40.

Wei, X, Dickman, MH and Pope MT (1997). *Inorg. Chem.*, **36**, 130–131.

Weinstein, S, Jahn, W, Hansen, HAS, Wittmann, HG and Yonath, A (1989). *Journal of Biological Chemistry*, **264**, 19 138–19 142.

Weinstein, S, Jahn, W, Glotz, C, Schlünzen, F, Levin, I, Janell, D, Harms, J, Kölln, I, Hansen, HAS, Glühmann, M, Bennett, WS, Bartels, H, Bashan, A, Agmon, I, Kessler, M, Pioletti, M, Avila, H, Anagnostopoulos, K, Peretz, M, Auerbach, T, Franceschi, F and Yonath, A (1999). *J. Struct. Biol.*, **127**, 141–151.

Wilson, KE and Noller, HF (1998). *Cell*, **92**, 337–349.
Wimberly, BT, White, SW and Ramakrishnan, V (1997). *Structure*, **5**, 1187–1198.
Yonath, A and Francschi, F (1998). *Structure*, **6**, 678–684.
Yonath, A, Harms, J, Hansen, HAS, Bashan, A, Schlünzen, F, Levin, I, Kölln, I, Tocilj, A, Agmon, I, Peretz, M, Bartels, H, Bennett, WS, Krumbholz, S, Janell, D, Weinstein, S, Auerbach, T, Piolleti, M, Morlang, S, Bhanumoorthy, P and Franceschi, F (1998). *Acta Crystallographica*, **A54**, 945–955.
Yonath, A, Leonard, KR and Wittmann, HG (1987). *Science*, **236**, 813–817.
Yonath, A, Glotz, C, Gewitz, HS, Bartels, S, von Böhlen, K, Makowski, I and Wittmann, HG (1988). *Journal of Molecular Biology*, **203**, 831–834.
Yonath, A, Harms, J, Hansen, HAS, Bashan, A, Peretz, M, Bartels, H, Schlünzen, F, Kölln, I, Bennett, WS, Levin, I, Krumbholz, S, Tocilj, A, Weinstein, S, Agmon, I, Piolleti, M, Janell, D, Auerbach, T and Franceschi, F (1998). *Acta Cryst.*, **54A**, 945–955.